Hybrid Silicon-Fiber Tunable Multi-Wavelength Laser with Switchable Frequency Spacing

Jean-Michel Vallée, Philippe Jean, and Wei Shi

IEEE Journal of Selected Topics in Quantum Electronics (2019)

Doi: 10.1109/JSTQE.2019.2938066

https://ieeexplore.ieee.org/document/8822793

Hybrid Silicon-Fiber Tunable Multi-Wavelength Laser with Switchable Frequency Spacing

Jean-Michel Vallée, Philippe Jean, Wei Shi, *Member, IEEE*

***Abstract*—Agile optical systems and elastic optical networks demand for flexible, high-performance laser sources. We demonstrate a hybrid silicon-fiber laser that can be largely tuned in wavelength, switched in frequency spacing and easily switched between multi- and single-wavelength operations. Single-mode laser with a fiber-coupled output power of 6 to 8 dBm was measured across the spectral range of 1545 nm to 1560 nm. No significant sign of power limitation from nonlinear absorption or free carrier generation in silicon was found. It is thus expected that a higher output can be obtained by improving the gain saturation performances as well as the fiber-to-chip coupling efficiency. For multi-wavelength operation, we have achieved a frequency spacing switchable between 56 GHz, 75 GHz, and 225 GHz. For both the multi- and single-wavelength operations, a linewidth of less than 20 kHz was measured. All the tuning mechanisms have been realized on the silicon chip, providing a scalable solution for tunable fiber lasers with minimized cost and integration complexity.**

***Index Terms*—Comb filters, Hybrid solution methods, Optical Fiber Lasers, Ring lasers, Silicon-on-insulator technology, Thermooptic effects, Tunable filters,**

I. Introduction

EMERGING optical systems in dynamic contexts demand for flexible, high-performance laser sources. For instance, application fields such as sensing and gas detection, wavelength division multiplexing (WDM) [1], light detection and ranging (LIDAR) and spectrum analysis [2] can largely benefit from highly tunable lasers. Elastic optical networks [3] require flexible coherent transceivers with both tunable data rate and bandwidth, for which multi-wavelength sources with tunability in both center wavelength and frequency spacing are of great interest for dynamic spectral resource allocation. For example, laser sources allowing switchable frequency spacing in the microwave region are of great interest for the development of the 5G technologies. Accordingly, a switchable spacing (10, 20, and 30 GHz) multi-wavelength fiber laser based on nonlinear effects was newly demonstrated [4].

In recent years, silicon photonics has been propelled as a leading technology in photonic integrated circuits (PIC). Its heading platform is the silicon-on-insulator (SOI) featuring 220-nm-thick wafers with a 2-μm buried oxide (BOX). The high optical confinement, the low propagation loss in telecommunications band, high volume and low-cost production, and the integration with electronic devices are responsible for the success of this technology. The potential of SOI-based light processing has allowed numerous filter designs with high quality factor (Q-factor) [5], extinction ratio (ER) and tuning performances. Such integrated cavities are highly desirable for the making of versatile tunable lasers. For instance, demonstrations of resonant silicon-based cavities using Vernier effect have shown widely tuned single-wavelength lasers [6], [7]. However, the indirect band-gap of the silicon hampers the material to accomplish efficient radiative recombinations which is a major hurdle to the full development of the functionalities of the silicon photonics. Thus, there have been considerable efforts focused on combining laser sources to the actual silicon platform.

Recent advances [8] in the heterogeneous integration of a direct band-gap III-V compound semiconductor on silicon platform as a gain medium for a laser source provide a promising solution. However, this approach still has to face a good number of challenges, such as thermal management and the complexity of the integration process (e.g. wafer bonding).

Alternatively, many all-fiber filters operated as comb cavities for a multi-wavelength laser operating at the C-band have been demonstrated. All-fiber lasers benefit from high-quality gain medium in doped fibers for high-power operation across a broad spectral window. Examples of all-fiber filter architectures include Lyot birefringent fiber filters [9], fiber Sagnac loop mirrors [10], Mach-Zehnder interferometers (MZI) [11], Fabry-Pérot filters [12] and chirped or sampled fiber gratings [13]. More recently, a single-multi-single (SMS) mode fiber interferometer allowing to the realization of a tunable-spacing (118 to 130 GHz) multi-wavelength laser was reported [14]. However, unlike silicon technology, the mature technology of optical fiber cannot achieve complex and highly flexible filter without relying on a complex architecture scheme. They require numerous optical components, which is bulky and subject to instabilities due to external perturbations such as temperature and vibrations [15].

While recent research effort was mainly focused on either all-fiber or III-V-silicon heterogeneous integration, there have been only a few demonstrations of hybrid silicon-based lasers with external erbium-doped fibers for passive [16] and active wavelength tuning using fiber elements [17] or an integrated filter on silicon [18]. Among the few demonstrations, there are two single-longitudinal-mode (SLM) erbium-doped fiber lasers incorporating a silicon-on-insulator (SOI) micro-ring resonator (MMR) as optical filter that were demonstrated. In the first case, the SLM was achieved by employing a saturable absorber [19] while it was achieved by employing a compound-ring architecture [20] in the other case. In both cases, a SOI MMR was used as fixed grid filter, and the

The authors are with the Centre d'optique, photonique et laser (COPL) and the Département de génie électrique et génie, Université Laval, Québec, QC, G1V 0A6, Canada.(e-mail: wei.shi@gel.ulaval.ca)

National Science and Engineering Research Council of Canada (NSERC) Funding: STPGP 494358-16

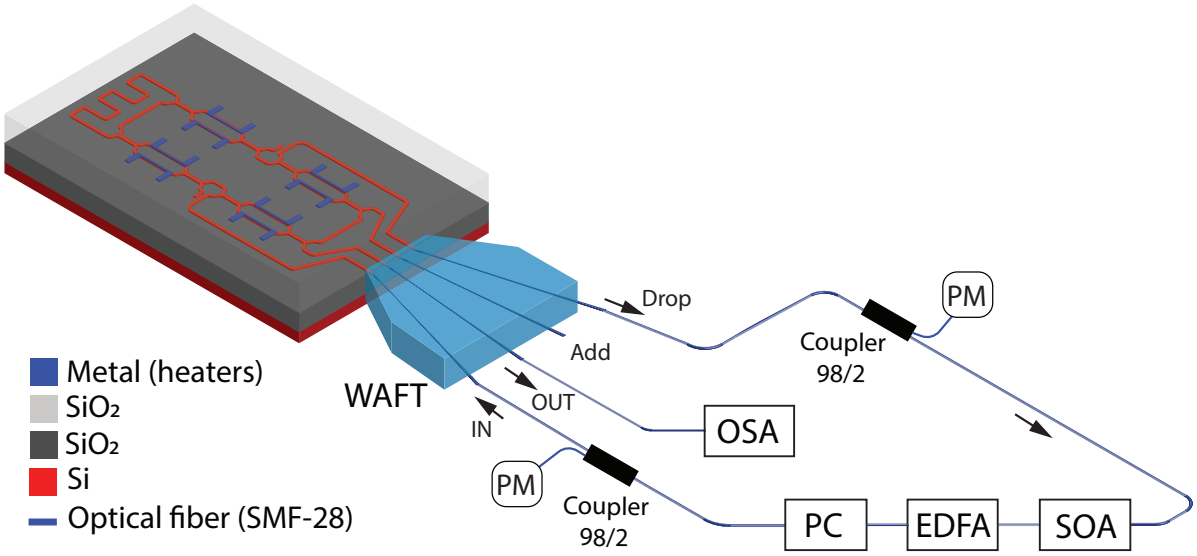

Fig. 1. Experimental set-up of the hybrid silicon-doped-fiber tunable laser: the fiber elements are edge-coupled to the silicon chip by a waveguide array fiber transposer (WAFT); the gain is provided by an Erbium doped fiber amplifier (EDFA) assisted by a semiconductor optical amplifier (SOA); the polarization is controlled with a polarization controller (PC); two power-meters (PM) are used to monitoring the circulating power in the cavity.

lasing wavelength selectivity was obtained by controlling the birefringent loss with a polarization controller. Furthermore, erbium-doped mode-locked ring fiber laser incorporating SOI MRR were also reported. The mode-locking mechanism was based either on a piece of highly nonlinear fiber [21] or via nonlinear broadening in the SOI MRR itself [22] and finally a phase modulator was added in the cavity to enhance the ER [23]. However, these hybrid laser prototypes were either only for single wavelength operation or with a fixed frequency spacing, and did not take advantage of the potential of light processing that the silicon photonics platform could offer.

In this paper, we present a flexible multi-wavelength laser, combining the merits of doped optical fibers and the flexible optical signal processing in silicon photonics. Here, the device presented can be easily switched between single-wavelength and multi-wavelength operations and offers tunable center wavelength as well as switchable frequency spacing. All the laser tuning mechanisms are realized on the silicon chip, allowing to reduce the number of optical components. The versatility of the design makes it likely to adapt the cavity to different types of rare-earth-doped fibers.

II. Modelling and Characterization of the Cavity

A schematic of our proposed hybrid silicon-fiber tunable laser is shown in Fig.1. A ring cavity is formed by bringing together the fiber elements required to provide the optical amplification and the silicon-based tunable filter. The ring cavity configuration was chosen instead of a standing-wave cavity because it eases the unidirectional oscillation for higher output power and better mode stability [24]. The laser tuning is achieved on the silicon chip using the Vernier effect between two nested resonant cavities with MZI-based thermo-optic switches.

A. Hybrid Laser cavity

As shown in Fig.1, the hybrid cavity consists of a silicon tunable filter, an erbium-doped fiber amplifier (EDFA), a polarization controller (PC), a semiconductor optical amplifier (SOA), and a Waveguide Array to Fiber Transposer (WAFT, provided by Teem Photonics) for the fiber to chip coupling with an insertion loss in the range of 1.5 to 2 dB per facet over the entire C-band. Two fused-fiber 2% couplers were positioned at the input and the output of the filter (see Fig.1) in order to monitor the injected power into the chip as well as the loss of the silicon-based intra-cavity filter. While set to optimize the Q-factor, the measured insertion loss of the filter, including the loss from the coupling is 9.5±1.0 dB. The total loss of the cavity for both the optical fiber elements ($\approx 1.5 \pm 0.5$ dB) and the silicon-based filter ($\approx 9.5 \pm 1.0$ dB) is approximately 11.0±1.5 dB. The uncertainty on the measures is mostly due to the mechanic-optical alignment in our experiment and can be significantly suppressed through optical packaging.

The total length of the ring cavity measured with an Optical Vector Analyzer (OVA) is 13.1 m, which gives a round-trip time (T_{rt}) of 64 ns with the assumption that the propagation is predominantly in silica fiber. The time delay for only the silicon-filter can be neglected since it is around 0.1 ns; this value was inferred from the measured Q-factor value of 5.7×10^4 of the passive silicon-based cavity (the Q-factor was obtained from the silicon filter transmission in Fig.3).

The expression of the Q-factor can be expressed by Eq.(1) [24]:

$$Q = \frac{2\pi c T_{rt}}{\lambda \delta_c}, \tag{1}$$

where δ_c is the losses per round-trip. Given the previously introduced T_{rt} and the total loss per round-trip of 11.0±1.5

National Science and Engineering Research Council of Canada (NSERC) Funding: STPGP 494358-16

dB, the Q-factor of the ring laser cavity can be estimated to be ranging from 2.7×10^7 to 3.6×10^7 at 1550 nm.

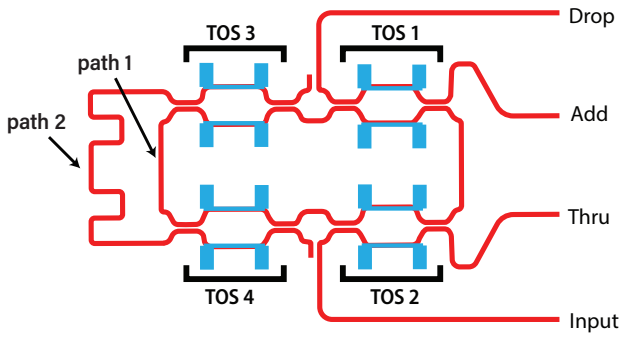

Fig. 2. Layout of the silicon-based filter formed by two nested cavities with the different paths (path 1 and path 2) .

B. Silicon-based filter

The schematic of the silicon-based filter is shown in Fig.2. The red paths represent the silicon waveguides and the blue elements are metallic elements acting as electrical heaters for the tuning. The device was designed based on a 220-nm-thick SOI wafer with a 2-μm buried oxide (BOX) and fabricated by AMF, Singapore via CMC Microsystems. The filter is made of two nested cavities, whose round-trip lengths are distinguished by the two paths labeled as path 1 and path 2. It is also comprising four balanced MZI used as thermo-optic switch (TOS).

The MZI-based TOSs allow to fully control losses and input/output (IO) coupling of the cavities by exploiting the thermo-optic effects in silicon. The TOS 3 and 4 control the coupling ratio between the two different paths (Path 1 and 2, corresponding to Cavity 1 and 2, respectively, in Fig. 2) while TOS 1 and 2 control the loss and coupling into the whole filter. The TOS has an insertion loss of less than 0.32 dB and consumes a power in a range of 18 mW to 22 mW for a π phase shift. More details on the design and characteristics of the TOS are presented in Appendix A.

The various paths of the filter that are highlighted in Fig.3 gives three different resonant cavities labeled as Cavity 1, Cavity 2 and Coupled Cavity. The round trip length for the shortest path (Cavity 1) and for the longest (Cavity 2) are respectively 775 μm and 1024 μm. Based on Vernier effect, an extended free spectral range (FSR) is obtained by setting the TOS 3 and 4 to equally couple the signal into both paths (Coupled Cavity).

The extended FSR is given by the following expression (2) :

$$\mathrm{FSR}_3 = \left|\frac{\mathrm{FSR}_2 \cdot \mathrm{FSR}_1}{\mathrm{FSR}_2 - \mathrm{FSR}_1}\right| = \frac{c}{ng}\left|\frac{1}{\Delta L_{1-2}}\right|, \qquad (2)$$

where $\mathrm{FSR}_{1,2}$ are the free spectral range of the nested ring cavity of path 1 and path 2, FSR_3 is the extended free spectral range, ng is the group index of the signal and ΔL_{1-2} is the difference of length between path 1 and path 2.

From Fig.3 we observe that the insertion loss of the silicon filter is around 5 dB (without fiber-to-chip coupling losses).

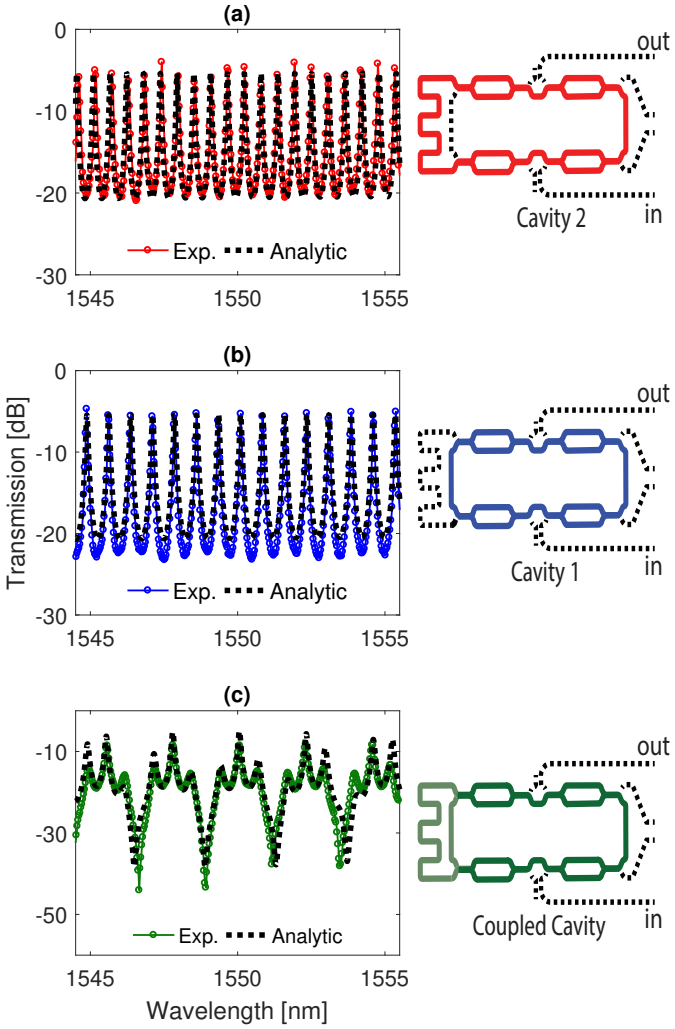

Fig. 3. Transmission at drop port of the filter for each cavity configurations : (a) Cavity 2, (b) Cavity 1; (c) both cavities (coupled cavity) for an extended FSR by the Vernier effect.

This relatively high insertion loss is a compromise as a result of optimizing the Q-factor values of the passive cavity, which are 5.7×10^4 (Fig.3a), 3.6×10^4 (Fig.3b) and 2.1×10^4 (Fig.3c) for Cavity 2, Cavity 1, and Coupled Cavity respectively.

The out-of-band rejection ratio for both Cavity 1 and 2 is around 16 dB. For the Coupled Cavity, the side-mode-suppression ratio (SMSR), i.e., the difference between the main peaks and their two adjacent side peaks, is ranging from 4 dB to 9 dB. However, as we will see in Section III, the SMSR can be significantly enhanced in laser operation.

An analytical model of the tunable silicon filter was realized using Scattering Matrix formalism [25]. The block diagram of the hybrid laser cavity used for the analytical model is shown in Fig.4. Each optical components that are represented by the blocks in Fig.4 was modelized with a 4×4 scattering matrix, and then a comprehensive solution was solved using Matlab. This modular method allows to eventually extend the model with additional nested cavities.

In Fig.3, the analytical solution (black-dotted curves) of the cavity for each wavelength-spacing configuration is compared

National Science and Engineering Research Council of Canada (NSERC) Funding: STPGP 494358-16

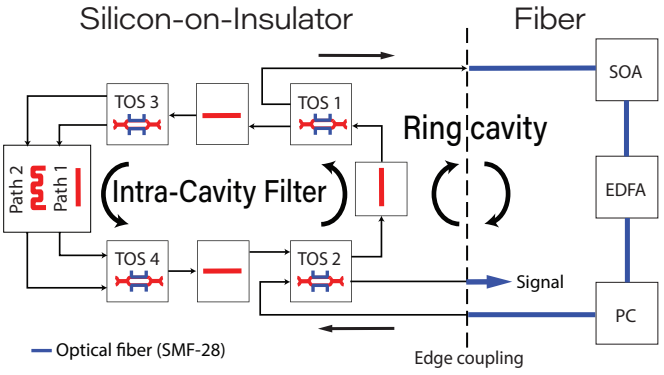

Fig. 4. Block diagram of the hybrid laser cavity.

to the experimental results (solid-colored curves). An excellent agreement is found between the experimental curves and the analytical model.

C. Gain

The optical amplification was provided by an EDFA (INO FAF-50) assisted by a SOA. The EDFA has a small-signal gain of 38 dB in its gain saturated regime. In such conditions, the saturated signal was approximately 15 dBm (see Appendix B).

A SOA was added to the cavity because of its inhomogeneous gain that allows suppressing mode competitions arising from erbium and thus increase the stability and the flatness of the laser. The SOA was also operating in the saturation regime with a saturated output signal of 12 dBm. Since the saturated output signal of the SOA was smaller than that of the EDFA, the SOA was placed before the EDFA to maximize the available circulating power. Note that the use of SOA was not mandatory and it could have been replaced by an integrated nonlinear stabilizer [26].

III. Experimental Results of Laser Operation

The tunable laser cavity, switchable between multi- and single-wavelength, was achieved by coupling the erbium-doped fiber with the silicon-based filter. The multi-wavelength laser operation was obtained by properly setting the cavity loss in varying the powers applied to the TOSs so that several longitudinal modes reach the lasing condition. The flexibility of the IO couplers (TOS 1 and TOS 2 in Fig.2) allows a trade-off between the loss and the Q-factor of the silicon filter.

Fig.5 shows the spectrum of the multi-wavelength laser centered at different wavelengths across C-band for each FSR configurations. The measured wavelength spacings are 0.45 nm, 0.60 nm and 1.80 nm (56 GHz, 75 GHz, and 225 GHz) for Cavity 1, Cavity 2, and Coupled Cavity (Fig. 3), respectively.

The number of excited modes per signal ranges between 4 and 7 and a flatness better than 3 dB of the four most significant laser lines was measured for all the configurations. The laser signal with 7 excited modes, represented in Fig.6, was obtained with the smallest wavelength spacing configurations (Cavity 2 in Fig.2). The peak power for the first 6 excited

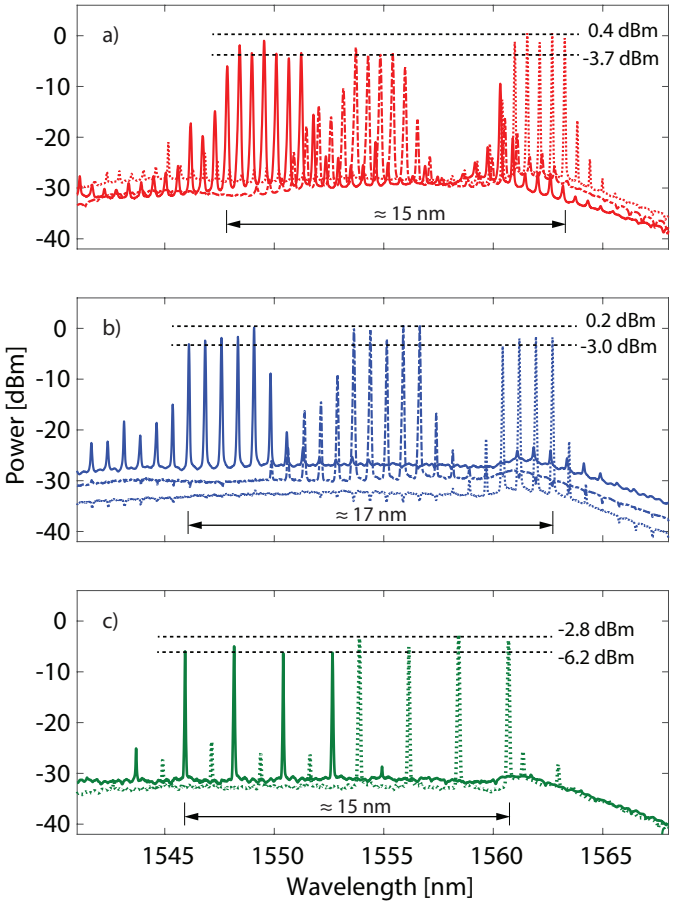

Fig. 5. Laser spectrum in multi-wavelength operation for different cavity configurations as shown in Fig. 2: (a) Cavity 2; (b) Cavity 1; (c) Coupled Cavity. The central wavelength is tunable between 1547 nm and 1563 nm by varying the powers applied to the heaters simultaneously: solid, dash-dotted, and dotted curves are for low power, medium power, and high power, respectively.

modes are ranging from -3.3 to -0.3 dBm; the 7th mode has a peak power of -5 dBm.

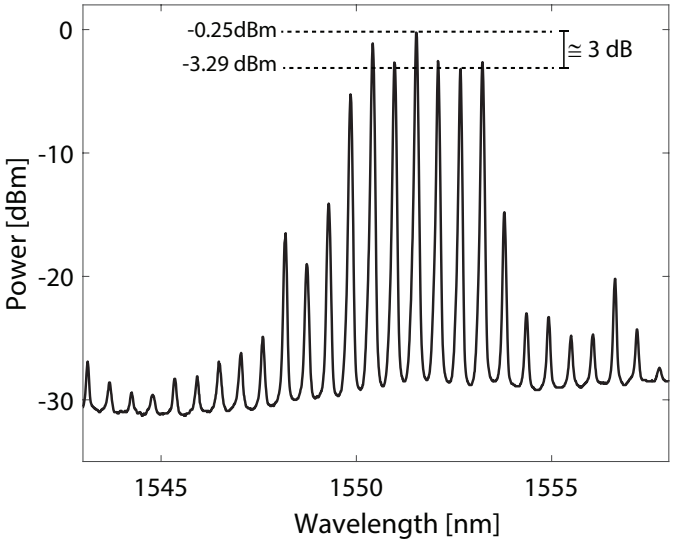

Fig. 6. Signal of a multi-wavelength laser with up to 7 excited mode and with an FSR of 0.45 nm.

National Science and Engineering Research Council of Canada (NSERC) Funding: STPGP 494358-16

For all the cavity configurations, a peak power between -5 dBm and 0.5 dBm was measured with an extinction ratio of >30 dB. The central wavelength of the spectrum could be tuned between 1545 nm and 1560 nm by thermally changing the phase of the cavity using the micro-heaters on the silicon chip.

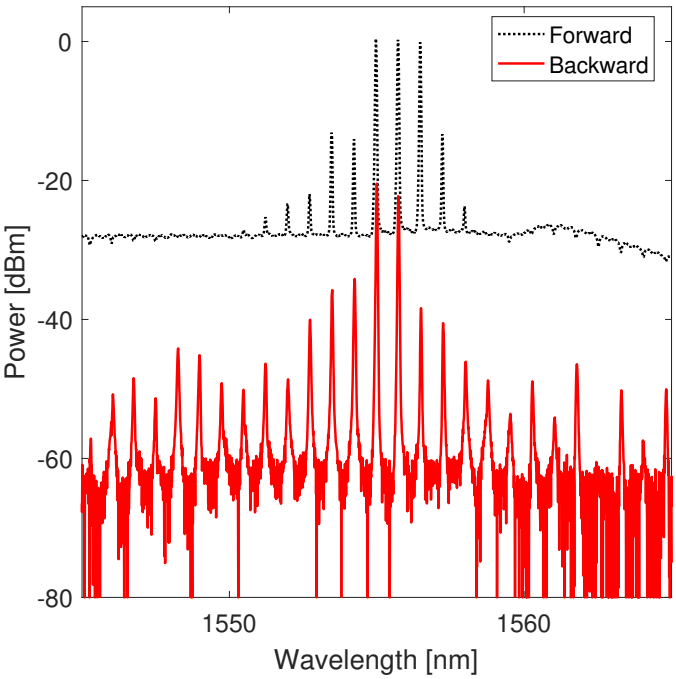

Fig. 7. Signal of the backward propagating signal (solid-red curve) and the forward propagating signal (dotted-black curve).

The backward-propagating signal in the cavity has also been investigated since optical unidirectional out-coupling laser light is fundamental in all-optical processing. The one direction propagation is possible thanks to non-reciprocal devices such as optical fiber isolators. Since integrating an optical isolator on silicon remains a great challenge due to the material incompatibility between semiconductor and magneto-optical materials [27], we have used the integrated optical isolator of the EDFA in order to inhibit the majority of the backward signal propagating in the cavity.

At the add port (see Fig.1), we measured a low-intensity contra-propagating signal that is mostly due to the backscattering effects in the silicon filter. In Fig.7, one sees the forward- and backward-propagating signals. While the strongest peak power of the forward signal is 0 dBm, we measured only -20 dBm for the peak of the contra-propagating signal. The extinction ratio (peak to background) for the backward signal is 42 dB against 30 dB measured for the forward signal.

The single-wavelength operation is obtained by increasing loss in the cavity by thermally tuning the TOSs so that only one mode reaches the threshold condition. Fig.8 shows the measured signal of the single-wavelength operation with an 8 dBm fiber-coupled peak power at 1553 nm, an extinction ratio >35 dB, and a SMSR of 31 dB. Changing the power applied to the heaters in the silicon filter, we tuned the center wavelength of the single mode laser from 1545 to 1560 nm and measured

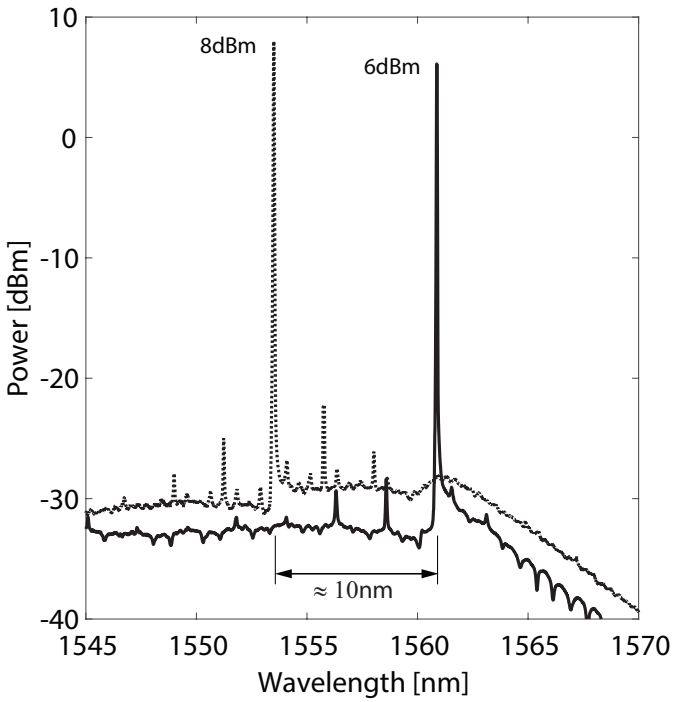

Fig. 8. Laser spectrum of the single-wavelength operation at 1553 nm and 1562 nm with a peak power of 8 dBm and 6 dBm and an SMSR of 31 dB and 36 dB, respectively.

an optical power larger than 6 dBm and an SMSR up to 40 dB.

The two 2% fiber couplers (Fig.1) were used to infer the overall SOI filter losses (including coupling losses with the fiber module). It was found that these losses did not depend on the optical signal level injected in the SOI (up to 14.5±0.5 dBm) meaning that at least up to this level, no sign of nonlinear absorption or free carrier generation was found. In fact, the signal output was more likely limited by the saturation level of the EDFA and SOA assembly. It is thus expected that a higher output could be obtained by improving the gain saturation performance of the EDFA or by improving the fiber-to-chip coupling loss.

We measured the stability for both the multi- and single-wavelength laser regimes. For the single-wavelength laser, the signal spectrum evolution over time is shown in Fig.9a whereas its measured peak power and center wavelength variation over a period of 15 min are shown in Fig.9b. Here, for an average output power of 5.50 dBm centered at 1550.45 nm, the standard deviations for both the output power and center wavelength were 0.27 dBm and 0.01 nm respectively.

As for the multi-wavelength laser operation (shown in Fig.10), the center wavelength of the 5 most significant peaks along with their standard deviation are 1558.99 ± 0.30 nm, 1559.76 ± 0.30 nm, 1560.51 ± 0.30 nm, 1561.27 ± 0.30 nm and 1562.10 ± 0.30 nm and their corresponding power fluctuations along with their standard deviation are -3.09 ± 0.72 dBm, -3.29 ± 0.62 dBm, -2.85± 0.49 dBm, -2.51 ± 0.82 dBm and -2.29 ± 0.97 dBm.

We measured the linewidth of the hybrid laser by using a delayed self-heterodyne method with a delay arm formed by

National Science and Engineering Research Council of Canada (NSERC) Funding: STPGP 494358-16

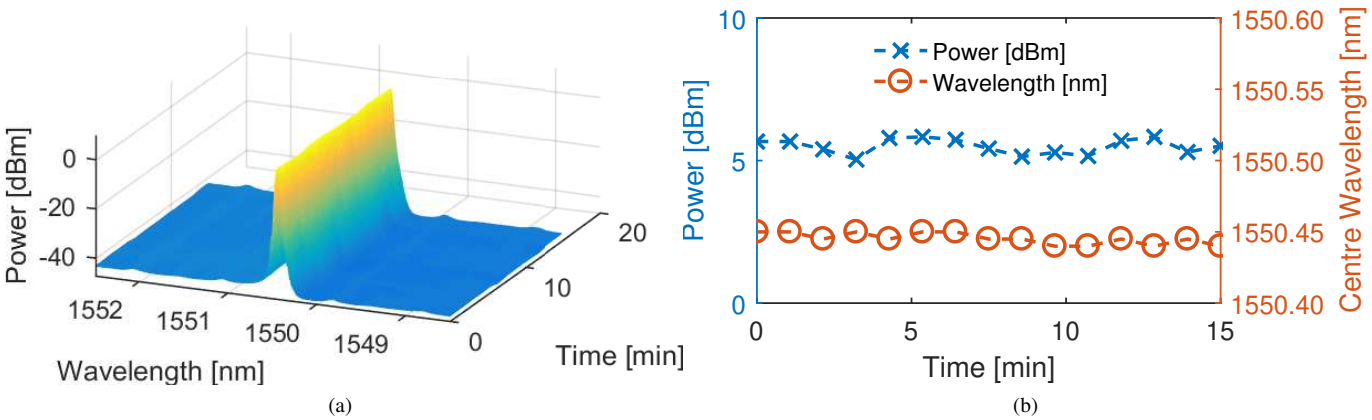

(a) (b)

Fig. 9. Power and wavelength stability as a function of the time (a) for the spectrum evolution (b) and for the measured peak power and center wavelength.

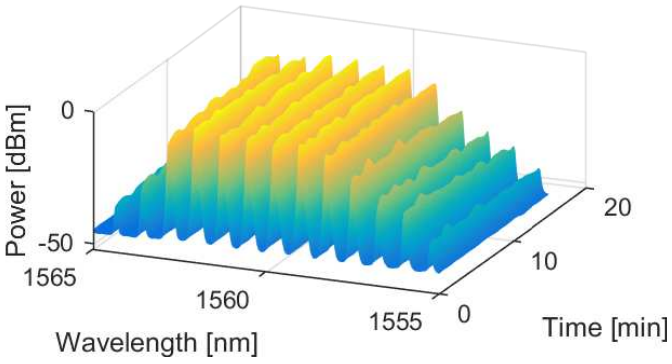

Fig. 10. Power stability as a function of the time for the multi-wavelength laser.

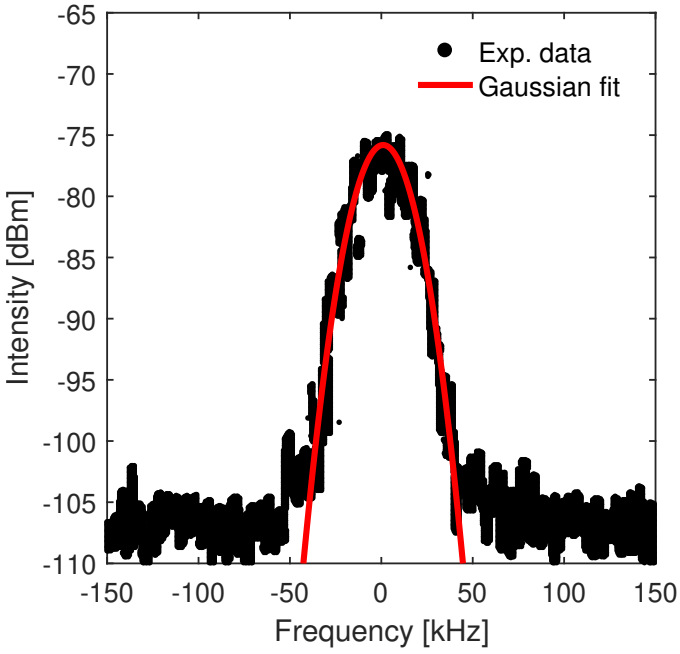

Fig. 11. Measured laser linewidth of 18 kHz from Gaussian curve-fitting in single-wavelength operation obtained by using delayed self-heterodyne method.

50 km of optical fiber and a phase modulator operating at 3 GHz on the other arm. The optical signal was converted to electrical signal by a 10 GHz photodiode and then analyzed by a 50 GHz RF spectrum analyzer. In doing so, we measured a linewidth of 18 kHz for the hybrid laser while running in single-wavelength regime. The linewidth corresponds to the full-width-half-max (FWHM) of a Gaussian curve-fitting as shown in Fig.11. The measured Gaussian line shape indicates that the linewidth is dominated by stochastic noise (e.g. thermal noise, instantaneous phase, vibrations, etc.) that broaden the natural Lorentzian linewidth of the laser.

IV. Conclusion

We have demonstrated a tunable hybrid ring laser with switchable frequency spacing formed by coupling a silicon-based flexible filter with an EDFA. The design of nested cavities with the Vernier effect allows the dynamically selected frequency spacing of a multi-wavelength laser, between 56 GHz, 75 GHz and 225 GHz. The number of excited modes per signal ranges between 4 and 7 and a flatness better than 3 dB for the four most significant laser lines was measured for all the configurations of the multi-wavelength laser. In single mode operation, we have obtained fiber-coupled peak power up to 8 dBm with a measured linewidth of 18 kHz.

Thanks to the scalability of silicon photonic circuits, we can further increase the number of possible configurations by increasing the number of nested cavities. Moreover, the tunable couplers of the filter allow to control the wavelength selectivity of the cavity and therefore to operate the laser either in the multi- or single-wavelength regime. This novel hybrid design makes the best use of mature silicon photonics and fiber processes, offering a solution for highly flexible, high-power lasers that may find crucial applications, e.g., for high-capacity optical transmissions and flexible optical networks.

Appendix A
Thermo-optic switch

The TOS is composed of two 3dB directional couplers and two arms with a length of 70 μm, each having an electrical heater for thermal control of the optical phase. The TOS is

National Science and Engineering Research Council of Canada (NSERC) Funding: STPGP 494358-16

illustrated in Fig.12a and its normalized transmission in dB as a function of the applied power in mW is shown in Fig.12b. We found that the π phase shift power is about 20 mW.

The analytical expression of the crossing transmission of a balanced MZI-based thermo-optic switch [28] that we used to fit with experimental data is given by:

$$T_{cross} = \frac{1}{2}\left(1 + \cos\left(\frac{-2\pi}{\lambda} \cdot L_{arm} \cdot dndT \cdot \Delta T\right)\right),$$

where L_{arm} is the length of one arm of the TOS, $dndT$ = 1.87×10^{-4} K^{-1} is the thermo-optic coefficient and ΔT is the temperature increase applied to one arm.

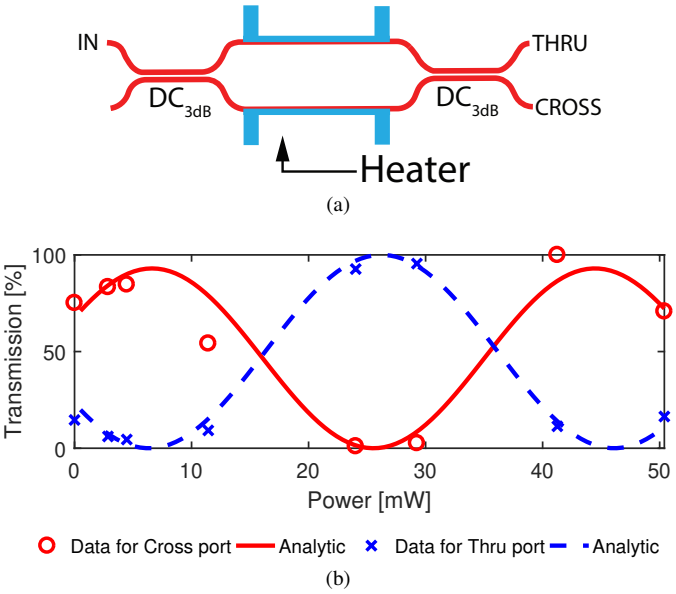

Fig. 12. (a) Schematic of the thermo-optic switch. (b) Transmission of the thermo-optic switch (TOS) as a function of the applied power.

Appendix B
Gain Parameters

The pump power of the INO FAF-50 Benchtop Erbium-Doped Fiber Amplifier was set to 200 mW for operating in gain saturated regime. In order to characterize the gain, a seed laser signal at 1550 nm was injected into the EDFA and the output signal was measured with a power-meter.

Both of the output power and the gain with respect to the input signal are shown in Fig.13a and Fig.13b, respectively. For input signals of -30 dBm and -4 dBm, we measured output powers of 8.0 dBm and 15.0 dBm, respectively. Under such conditions, a small-signal gain of 38 dB was inferred.

Acknowledgment

This project is supported by the Natural Sciences and Engineering Research Council of Canada (STPGP 494358 - 16) and by the "Fond de recherche du Québec-Nature et technologies (FRQNT)". We thank CMC Microsystems for the fabrication subsidy. We also thank Professor Michel Piché who provided expertise that greatly assisted the project.

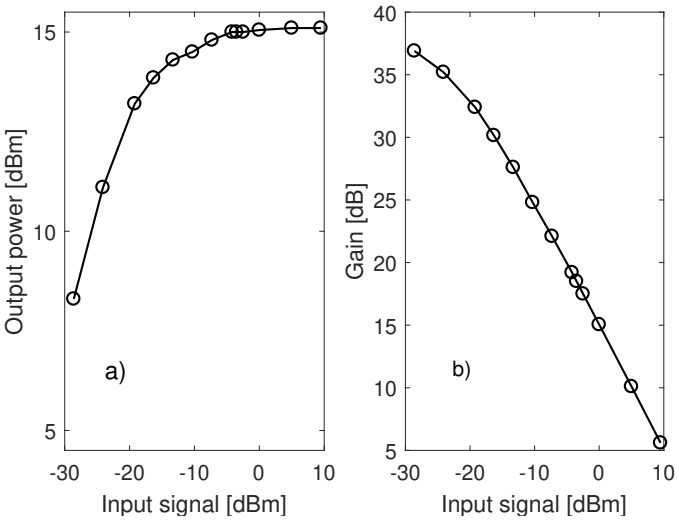

Fig. 13. Characterization of (a) the output power and (b) the gain of the EDFA as a function of the injected laser signal at 1550 nm.

References

[1] D. Liu, Q. Sun, P. Lu, L. Xia, and C. Sima, "Research progress in the key device and technology for fiber optic sensor network," Photonic Sensors, vol. 6, no. 1, pp. 1–25, Mar. 2016.

[2] R. Rossi, J.-F. Ciparisse, A. Malizia, M. Gelfusa, and P. Gaudio, "Multiwavelength differential absorption lidar to improve measurement accuracy: test with ammonia over a traffic area," Applied Physics B, vol. 124, no. 7, Jul. 2018.

[3] O. Gerstel, M. Jinno, A. Lord, and S. J. Yoo, "Elastic optical networking: a new dawn for the optical layer?," IEEE Communications Magazine, vol. 50, no. 2, pp. s12–s20, Feb. 2012.

[4] N. A. Bt Ahmad, S. H. Dahlan, N. A. Cholan, H. Ahmad, and Z. C. Tiu, "Switchable 10, 20, and 30 GHz region photonics-based microwave generation using thulium-doped fluoride fiber laser," Journal of the Optical Society of America B, vol. 35, no. 7, p. 1603, Jul. 2018.

[5] Y. Zhang et al., "Design and demonstration of ultra-high-Q silicon microring resonator based on a multi-mode ridge waveguide," Optics Letters, vol. 43, no. 7, p. 1586, Apr. 2018.

[6] Y. Zhang et al., "Quantum dot SOA/silicon external cavity multi-wavelength laser," Optics Express, vol. 23, no. 4, p. 4666, Feb. 2015.

[7] A. Verdier et al., "Ultrawideband Wavelength-Tunable Hybrid External-Cavity Lasers," Journal of Lightwave Technology, vol. 36, no. 1, pp. 37–43, Jan. 2018.

[8] J. E. Bowers et al., "Realities and challenges of III-V/Si integration technologies," in Proc. Opt. Fiber Commun. Conf. Exhibit., San Diego, California, CA, USA, 2019, pp. 1–3.

[9] Young-Geun Han, Gilhwan Kim, Ju Han Lee, Sang Hyuck Kim and Sang Bae Lee, "Lasing wavelength and spacing switchable multiwavelength fiber laser from 1510 to 1620 nm," IEEE Photonics Technology Letters, vol. 17, no. 5, pp. 989–991, May 2005.

[10] S. Wang, M. Lv, Y. Zhang, and X. Chen, "Wavelength-spacing-controllable multi-wavelength fiber laser based on a Lyot–Sagnac filter," Applied Optics, vol. 57, no. 30, p. 8845, Oct. 2018.

[11] Y.-W. Zhou and G.-Y. Sun, "Optically tunable multiwavelength fiber laser based on a Mach–Zehnder comb filter incorporating ytterbium-doped fibers," Laser Physics, vol. 28, no. 1, p. 015105, Jan. 2018.

[12] J. Gutierrez-Gutierrez et al., "Switchable and multi-wavelength linear fiber laser based on Fabry–Perot and Mach–Zehnder interferometers," Optics Communications, vol. 374, pp. 39–44, Sep. 2016.

[13] X. Zhao, M. Dong, Y. Zhang, F. Luo, and L. Zhu, "Switchable multi-wavelength and tunable wavelength spacing erbium-doped fiber laser based on a phase-shifted fiber Bragg grating combined with a Mach-Zehnder interferometer," Optics & Laser Technology, vol. 112, pp. 500–507, Apr. 2019.

[14] H. Ahmad, S. I. Ooi, and Z. C. Tiu, "100 GHz free spectral range-tunable multi-wavelength fiber laser using single–multi–single mode fiber interferometer," Appl. Phys. B, vol. 125, no. 6, p. 99, May 2019.

[15] R. A. Perez-Herrera, S. Chen, W. Zhao, T. Sun, K. T. V. Grattan, and M. López-Amo, "Experimental Optimization in Terms of Power Stability

and Output Power of Highly Erbium-Doped Fiber Lasers with Single and Hybrid Cavities," Fiber and Integrated Optics, vol. 29, no. 2, pp. 106–120, Mar. 2010.
[16] L. G. Yang, C. H. Yeh, C. Y. Wong, C. W. Chow, F. G. Tseng, and H. K. Tsang, "Stable and wavelength-tunable silicon-micro-ring-resonator based erbium-doped fiber laser," Opt. Express, OE, vol. 21, no. 3, pp. 2869–2874, Feb. 2013.
[17] C. Yeh, H. Cheng, Y. Chang, C. Chow, and J. Chen, "Silicon-Micro-Ring Resonator-Based Erbium Fiber Laser With Single-Longitudinal-Mode Oscillation," IEEE Photonics Journal, vol. 10, no. 3, pp. 1–7, Jun. 2018.
[18] N. Li et al., "C-band swept wavelength erbium-doped fiber laser with a high-Q tunable interior-ridge silicon microring cavity," Opt. Express, OE, vol. 24, no. 20, pp. 22741–22748, Oct. 2016.
[19] Y. Hsu, C.-H. Yeh, C.-W. Chow, Y.-C. Chang, and H.-Y. Cheng, "Stabilized single-longitudinal-mode erbium fibre laser employing silicon-micro-ring resonator and saturable absorber," Laser Phys., vol. 28, no. 7, p. 075103, May 2018.
[20] Y. Hsu, C.-H. Yeh, H.-Y. Cheng, Y.-C. Chang, and C.-W. Chow, "Employment of silicon-micro-ring resonator and compound-ring architecture for stable and tunable single-longitudinal-mode fiber laser," Optics & Laser Technology, vol. 105, pp. 114–117, Sep. 2018.
[21] S. Jyu et al., "250-GHz Passive Harmonic Mode-Locked Er-Doped Fiber Laser by Dissipative Four-Wave Mixing With Silicon-Based Micro-Ring," IEEE Photonics Journal, vol. 5, no. 5, pp. 1502107–1502107, Oct. 2013.
[22] L.-G. Yang et al., "A 110 GHz passive mode-locked fiber laser based on a nonlinear silicon-micro-ring-resonator," Laser Phys. Lett., vol. 11, no. 6, p. 065101, 2014.
[23] Y. Liu et al., "110 GHz hybrid mode-locked fiber laser with enhanced extinction ratio based on nonlinear silicon-on-insulator micro-ring-resonator (SOI MRR)," Laser Physics Letters, vol. 13, no. 3, p. 035101, Mar. 2016.
[24] A. E. Siegman, Lasers. Mill Valley, California: University Science Books, 1986.
[25] W. Shi, R. Vafaei, M. Á. G. Torres, N. A. F. Jaeger, and L. Chrostowski, "Design and characterization of microring reflectors with a waveguide crossing," Optics Letters, vol. 35, no. 17, p. 2901, Sep. 2010.
[26] H. Ahmad, N. A. Hassan, S. N. Aidit, and Z. C. Tiu, "Generation of tunable multi-wavelength EDFL by using graphene thin film as nonlinear medium and stabilizer," Optics & Laser Technology, vol. 81, pp. 67–69, Jul. 2016.
[27] L. Bi et al., "On-chip optical isolation in monolithically integrated non-reciprocal optical resonators," Nature Photonics, vol. 5, no. 12, pp. 758–762, Dec. 2011.
[28] L. Chrostowski and M. Hochberg, "Modulators," in Silicon Photonics Design: From Devices to Systems, Cambridge: Cambridge University Press, 2015, pp. 217–258.

Jean-Michel Vallée received the B.E. degree in engineering physics in 2018 from the Université Laval, Québec, QC, Canada, where he is currently working towards the M.S. degree in electrical engineering at the Centre d'Optique, Photonique et Laser. His research interests include silicon photonics, tunable filters and lasers.

Philippe Jean received the B.E. degree in engineering physics in 2015 from the Université Laval, Québec, QC, Canada, where he is currently working towards the Ph.D. degree. His research interests include silicon photonics, lasers and integrated chalcogenides for the MIR.

Wei Shi (S'07-M'12) is an Associate Professor in the Department of Electrical and Computer Engineering, Université Laval, Québec, QC, Canada. He received the Ph.D. degree in electrical and computer engineering from the University of British Columbia, Vancouver, BC, Canada, in 2012, where he was awarded the BCIC Innovation Scholarship for a collaboration entrepreneurship initiative. Before joining Université Laval in 2013, he was a researcher at McGill University, Montreal, QC, Canada, where he held a Postdoctoral Fellowship from the Natural Sciences and Engineering Research Council of Canada (NSERC). He is currently an Associate Professor with the Department of Electrical and Computer Engineering, Université Laval, Québec, QC, Canada. His current research focuses on integrated photonic devices and systems, involving silicon photonics, nanophotonics, CMOSphotonics co-design, high-speed optical communications, chip-scale lasers, and optical sensors. He is a member of the Center for Optics, Photonics and Lasers (COPL) and holds a Canada Research Chair in Silicon Photonics.

National Science and Engineering Research Council of Canada (NSERC) Funding: STPGP 494358-16